J_{eff} states in quasi-one-dimensional antiferromagnetic spin chain hexagonal iridates Sr_3MIrO_6 (M=Mg, Zn, Cd): An *ab initio* comparative perspective

Roumita Roy [*] and Sudipta Kanungo [†]
School of Physical Sciences, Indian Institute of Technology Goa, Goa-403401, India

(Received 11 August 2023; revised 26 December 2023; accepted 19 January 2024; published 6 February 2024)

We employ first-principles density-functional theory to perform a comparative investigation of the effect of the spin-orbit coupling (SOC) on the electronic and magnetic properties of three experimentally synthesized and characterized hexagonal perovskites Sr_3MIrO_6 (M = Mg, Zn, Cd). The electronic-structure calculations show that in all compounds, Ir is the only magnetically active site in the $+4[5d^5]$ configuration, whereas M^{+2} (M = Cd, Zn, Mg) remains in nonmagnetic states with Cd/Zn and Mg featuring d^{10} and d^0 electronic configurations, respectively. The insulating gap could be opened by switching on the correlation parameter U for Sr_3CdrO_6 and Sr_3ZnIrO_6, which qualifies it to be a correlated Mott insulator. However, in the case of Sr_3MgIrO_6, both U and antiferromagnetic ordering is not enough and the gap could only be opened by including the SOC, which classifies it to fall under the category of a typical SOC Mott insulator. The j_{eff} states are visualized from the orbital-projected band structure. The magnetism is studied from the point of view of exchange interactions and magnetocrystalline anisotropy in the presence of the SOC. We also present the comparative analysis of the renormalized impact of SOC on the three compounds, which shows that all three compounds fall under the intermediate coupling regime, where Sr_3MgIrO_6 is comparatively closer to the atomic $j_{\text{eff}} = \frac{1}{2}$ picture from the others.

DOI: 10.1103/PhysRevB.109.085107

I. INTRODUCTION

Iridates provide a fertile ground to understand the delicate interplay among various energy scales that include Coulomb correlation, Hund's coupling, crystal-field splitting, exchange interactions, bandwidth, and spin-orbit coupling (SOC). While the last decade has seen a major boom in studies revolving around iridates [1–5], the major thrust was provided by celebrated work on Sr_2IrO_4 [6,7], where SOC Mott insulating state was shown in the octahedral environment of Ir by the combined effect of the strong SOC and the Hubbard U, as a result the supposedly half-filled band split into $j_{\text{eff}} = \frac{1}{2}$ lower and upper Hubbard bands. This further allows us to study the magnetism of such systems in terms of the new good quantum number j, as derived from the atomic j-j coupling description [8–13] in the presence of the local uniform octahedral environment.

Interestingly, the common notion is that the half-filled iridates belong to the strong SOC regime, where the atomic j-j coupling prescription would be the most suitable description and the emergence of the j_{eff} state is contemplated to be an obvious phenomenon. However, inside the solid in the noncubic crystal field environment, the atomic SOC can be screened heavily and the effective renormalized strength of SOC is not always sufficient to derive the anticipated j_{eff} states in iridates. The pentavalent iridates in $5d^4$ sconfiguration is expected to show $j_{\text{eff}} = 0$ nonmagnetic state [14,15] per the atomic j-j coupling descriptions. However, in the last few years, there have been several studies on Ba_2YIrO_6, Sr_2YIrO_6, Sr_2GdIrO_6 [13], $Ba_3ZnIr_2O_9$ [16], $Ba_2YSb_{1-x}Ir_xO_6$ [17], and $Sr_3(Li/Na)IrO_6$ [18,19] across several compositions of the iridates which reveals the breakdown of the $j_{\text{eff}} = 0$ picture. This may be because of the dominance of Hund's coupling over SOC [4], band structure [13], noncubic crystal field [17], quantum spin fluctuation [19], or effective normalization of the SOC due to the spin [20], and in all these cases the key factor is the strong competition among multiple energy scales in the case of iridates.

For tetravalent iridates in the $5d^5$ ($S = \frac{1}{2}$) state, the effective SOC strength is comparatively higher than its pentavalent $5d^4$ ($S = 1$) counterpart. This allows for the competition among the different scales to be even tighter between $S = \frac{1}{2}$ (atomic $L - S$ coupling) and $j_{\text{eff}} = \frac{1}{2}$ (atomic j-j coupling) descriptions. However, even in the tetravalent iridates, there are several reports on Sr_2CeIrO_6 [21] and Sr_3CuIrO_6 [22,23], which reveal strong mixing between $j_{\text{eff}} = \frac{1}{2}$ and $j_{\text{eff}} = \frac{3}{2}$ in addition to the competing energy scales of the exchange interactions, bandwidth, and mixing of t_{2g}-e_g orbitals [24], thus the atomic $j_{\text{eff}} = \frac{1}{2}$ state description is not completely valid. Hence, the impact of SOC cannot be generalized within this family of iridates and one should not decide the effect of SOC in deriving the j_{eff} states on general grounds by looking at the nominal electronic valence state only.

In the present paper, we have considered the hexagonal perovskites family of compounds with the general formula $A_3BB'O_6$, where the A site is an alkaline earth metal, and the B and B' sites belong to the transition metals and are the magnetic sites. The available literature on this family is vast due to the tunability of A, B, and B' sites. Popular choices for the A site include Sr and Ca. With Sr, there are

[*] roumita19221103@iitgoa.ac.in
[†] sudipta@iitgoa.ac.in

examples of magnetic excitation [25,26], Griffiths-phase-like behavior [27], noncollinear magnetism [28], and classical spin-liquid behavior [29] reported in the literature. While with the latter, i.e., Ca, we have reports of antiferromagnetic insulator [30], partially disordered antiferromagnetic phase [31], superparamagnetic clusters [32], multiferrocity [33], and so on. What makes these systems even more interesting is that the effective structural dimensionality of the system is lower than three dimensions. The structure comprises alternating, face-shared BO_6 trigonal prism and $B'O_6$ octahedra connected in a chainlike fashion along the crystallographic c axis. The transition metal sublattice forms a hexagonal arrangement in the ab plane and hence the nomenclature. The presence of isolated spin chains with localized magnetic moments provides an ideal ground to manifest low-dimensional magnetism with a prominent signature of quantum fluctuations for small effective spin systems. Our primary focus is on systems where the B' site is occupied by an Ir atom so the investigation of j_{eff} states can be realized in the strong SOC limit. While hexagonal perovskites have been discussed a lot in the context of low-dimensional spin systems, nevertheless, the rise of SOC-driven j_{eff} states in the presence of low dimensionality is yet to be explored in detail. A few examples of such hexagonal iridates found in the literature include Sr_3CuIrO_6 [22], Sr_3CoIrO_6 [34], Sr_3NiIrO_6 [35,36], Sr_3NaIrO_6 [19], and Sr_3LiIrO_6 [15]. Note that $Sr_3(Na/Li)IrO_6$ [15] and $Sr_3(Ni/Co)IrO_6$ [37] are believed to depict the $j_{\text{eff}} = \frac{1}{2}$ state at the Ir site, however, very recent studies [18,19,22,23] show that Ir is no longer in the atomic j-j coupling regime. Therefore, a detailed material-specific electronic structure investigation is indispensable to understand the effective impact of SOC in deriving the electronic structure. This makes our current work even more relevant where a material-specific description is portrayed that highlights the impact of SOC in the compound, from the microscopic point of view.

In the current paper, we perform a comparative study of the electronic and magnetic properties of three experimentally synthesized and characterized hexagonal iridates: Sr_3CdIrO_6 (SCIO), Sr_3ZnIrO_6 (SZIO), and Sr_3MgIrO_6 (SMIO) [38,39]. As per previous experiments, all three compounds show antiferromagnetic ordering. The transition temperatures are reported to be 22 K and 19 K for SCIO and SZIO, respectively [38], whereas in the case of SMIO the susceptibility vs temperature curve shows maxima at 13 K, however, the exact value of T_N is inconclusive [39]. Further extensive microscopic analysis on SZIO predicts the T_N to be of the order of 17 K [40,41]. In this paper, we perform a relative analysis of the electronic structure and properties of these three compounds and address the pertinent question about the diversified impact of SOC on different materials belonging to the iridate family. Our initial study includes analyzing the structural and electronic properties of these three systems, which reveals that Ir in the $+4[5d^5]$ configuration is the only magnetically active site, whereas Cd, Zn, and Mg remain inactive with an inert configuration. The point to be noted here is that in this situation we are dealing with two extremities with nonmagnetic Zn/Cd in closed shell (d^{10}) and Mg in open shell (d^0) configurations. Our study is crucial to realize the evolution of magnetism and the effect of SOC in these isostructural and isoelectronic hexagonal iridates by modification at only the nonmagnetic sites which apparently should not modify the influence of SOC. Our study microscopically reveals the fact that SMIO falls under the category of the relativistically driven Mott insulator with large magnetocrystalline anisotropy (MCA) energy, whereas SCIO and SZIO are correlation-driven Mott insulators This is driven by the complex energy landscapes involving electronic correlation, bandwidth, crystal field splitting, and SOC. In the following sections, we reveal that although the three compounds lie in the intermediate regime of complete L-S and j-j coupling schemes, the footprints of SOC are found to be very material-specific.

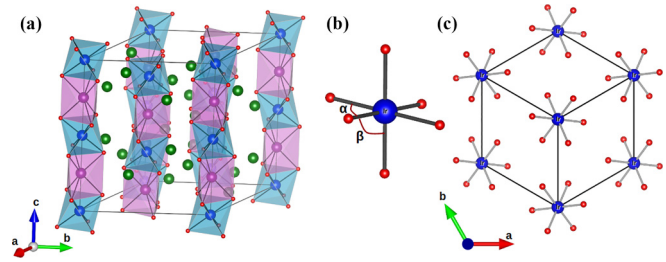

FIG. 1. (a) Crystal structure of Sr_3MIrO_6 (M = Mg, Zn, Cd). The Sr, M, Ir, and O atoms are represented by green. violet, blue, and red spheres, respectively. The IrO_6 octahedra and the MO_6 trigonal prism is shown in blue and violet polyhedras, respectively. (b) IrO_6 octahedra. (c) Hexagonal arrangement of Ir sublattice as seen from the chain direction.

II. CALCULATION METHODOLOGY

The DFT calculations were performed within the plane-wave based basis set of 500 eV cutoff on a pseudopotential framework with Perdew-Burke-Ernzerhof [42] exchange-correlation functional as implemented in the VIENNA AB INITIO SIMULATION PACKAGE [43,44]. The effect of electron-electron Coulomb correlations for the Ir-5d states was taken into account via on-site Hubbard U ($U_{\text{eff}} = U$-J$_H$) [45,46]. The SOC effect has been incorporated in the calculations through relativistic corrections to the original Hamiltonian [47]. We used $5 \times 5 \times 3$ k-mesh in the Brillouin zone for the self-consistent calculations. The experimentally obtained structures were optimized by relaxing the atomic positions towards equilibrium until the Hellmann-Feynman force becomes less than 0.001 eV/Å, keeping the lattice parameters fixed at the experimentally obtained values.

III. CRYSTAL STRUCTURE

The three hexagonal iridates under discussion have a K_4CdCl_6-type structure in the rhombohedral space group ($R\bar{3}c$). For the conventional crystal structure, the Sr, M, Ir, and O atoms occupy the 18e(x, 0, 0.25), 6a (0, 0, 0.25), 6b (0, 0, 0), and 36f (x, y, z) Wyckoff positions, respectively. Figure 1(a) shows the linear 1D chainlike arrangement of the face-shared IrO_6 octahedra and the MO_6 trigonal prism, thus forming a Ir-M-Ir-M chainlike structure along the global c direction with the Ir-M-Ir angle being 180°. The point to be noted here is that the above-mentioned consecutive Ir-M-Ir-M chains are

TABLE I. Experimental and theoretically optimized atomic internal coordinates for Sr and O atoms. The lattice constant was kept fixed at experimentally obtained values as reported in Refs. [38,39].

		Lattice constant (Å)		Sr	O		
Compound	Method	a	c	x	x	y	z
SMIO	expt.	9.666	11.103	0.364	0.174	0.023	0.113
	GGA+U			0.365	0.173	0.021	0.116
SZIO	expt.	9.633	11.203	0.363	0.172	0.020	0.112
	GGA+U			0.364	0.174	0.020	0.113
SCIO	expt.	9.657	11.604	0.362	0.173	0.018	0.107
	GGA+U			0.363	0.180	0.022	0.105

not connected among each other, so effectively the crystal structure can be considered to consist of a collection of virtual 1D chains. The IrO_6 octahedras are slightly tilted towards the $a-b$ plane, such that the global z axis doesn't coincide with the octahedral axis. The Sr atoms lie within the hollow space in between the linear chains. The hexagonal arrangement of Ir atoms can be visualized in Fig. 1(b). The lattice parameters and atomic coordinates for Sr_3MgIrO_6 (SMIO), Sr_3ZnIrO_6 (SZIO), and Sr_3CdIrO_6 (SCIO) are mentioned in Table I. The lattice constant along the global c axis increases with the increase in the radius of the M atom from Mg to Cd. We find that post structural optimization of the atomic positions of the M and Ir sites do not alter from the experimental Wyckoff positions. Even in the case of Sr and O atoms, the structure doesn't deviate much from the experimental case. Table II lists selected bond lengths and bond angles for the three compounds. Within the IrO_6 octahedra, the bond lengths are equal. However, the bond angles deviate from the ideal 90°, which causes the Ir-5d orbitals to experience a noncubic crystal field. This distortion is more pronounced in the case of SMIO than SZIO, followed by SCIO. This trend is consistent with the ionic radius of the M^{2+} ions, which is smallest for Mg^{2+}, followed by Zn^{2+} and Cd^{2+}.

IV. ELECTRONIC STRUCTURE

Figures 2(a)–2(c) show the GGA+U ($U_{\text{eff}} = 2$ eV) orbital projected DOS for all the three compounds. In all three cases, the Sr dominated bands lie far away from the Fermi energy and are not shown within the energy range. Sr is in an inert state with a valency of +2, with no major contribution to the DOS at E_f. In the case of SCIO and SZIO, the Cd-4d and Zn-3d states, respectively, are completely filled in both spin channels. For SZIO, the Zn states lie 6 eV below the E_f whereas for SCIO the Cd states lie even farther, i.e., ≈8 eV below the E_f. This is in conformity with Zn and Cd being in +2 valence states. On a similar footing, Mg in SMIO is in +2 valence state with completely empty d orbitals. The DOS lying between −6 to −4 eV arises from the strong hybridization between the Ir-5d and O-2p states, as reflected from Figs. 2(a)–2(c). The O-2p DOS is mainly concentrated within the energy range −4 to −1 eV and is well separated from the Ir-5d states near the Fermi energy, in the case of SZIO and SMIO. In the octahedral environment, the Ir-5d states split into t_{2g} and e_g states, with the e_g states being completely empty in both the spin channels and can be seen in Figs. 2(a)–2(c) in the energy range of 3 to 4 eV. The t_{2g} states are completely filled in the majority spin channel and partially filled in the minority spin channel. The values of the spin magnetic moment are listed in Table III. We find that the moment at the Ir site increases as we move from SMIO to SCIO. The net moment for all three systems is found to be 1 μ_B per formula unit. Looking at the combined results of DOS and the magnetic moment we conclude that Ir is in +4[$5d^4$] with a low spin state of $S = \frac{1}{2}$ in all three compounds. The absence of a substantial value of moment at the O site further suggests that the magnetic moment at the Ir site is quite localized. Thus, this system can be considered to be an arrangement of spin-$\frac{1}{2}$ linear chains running along the c direction. The interactions within this chain and with its neighboring ones are discussed in subsequent sections. Furthermore, as compared to other iridates [6], the bandwidth of the t_{2g} states here is much narrower due to reduction in the electronic hopping as a result of lower structural connectivity. Thus, it is natural to expect that it would be possible to open the insulating gap with the inclusion of a reasonable value of on-site Hubbard U. Counterintuitively, the insulating nature is only possible with U value of 2 eV for the SCIO as seen in Figs. 2(c) and 2(f). On the other hand, for SZIO, a larger value of $U = 3$ eV is required to open the gap as evident in Figs. 2(b) and 2(e). We believe that the increased structural distortion in SZIO, as compared to SCIO, calls for a larger value of U in SZIO to open up this gap. While a marginal gap opens at the Fermi energy for SCIO and SZIO for U values of 2 eV and 3 eV, respectively, SMIO essentially retains its metallic character with a large U value even up to 4 eV at the Ir site. Furthermore, it is widely known that on imposing the AFM order, it is possible to open a band due to a reduction in bandwidth. Nevertheless, even with the introduction of antiferromagnetic ordering, SMIO holds its metallic state in the spin-down channel as can be seen in Fig. 2(d).

Figures 3(a) and 3(b) show the GGA+FM+SOC and GGA+U+FM+SOC band structures for SMIO, respectively,

TABLE II. Bond lengths (Å) and bond angles (°) for theoretically optimized crystal structure for SMIO, SZIO, and SCIO.

	SMIO	SZIO	SCIO
Ir-O	2.04	2.03	2.05
M-O	2.17	2.20	2.35
O-Ir-O (α)	84.41	85.08	87.96
O-Ir-O (β)	95.58	94.92	92.04

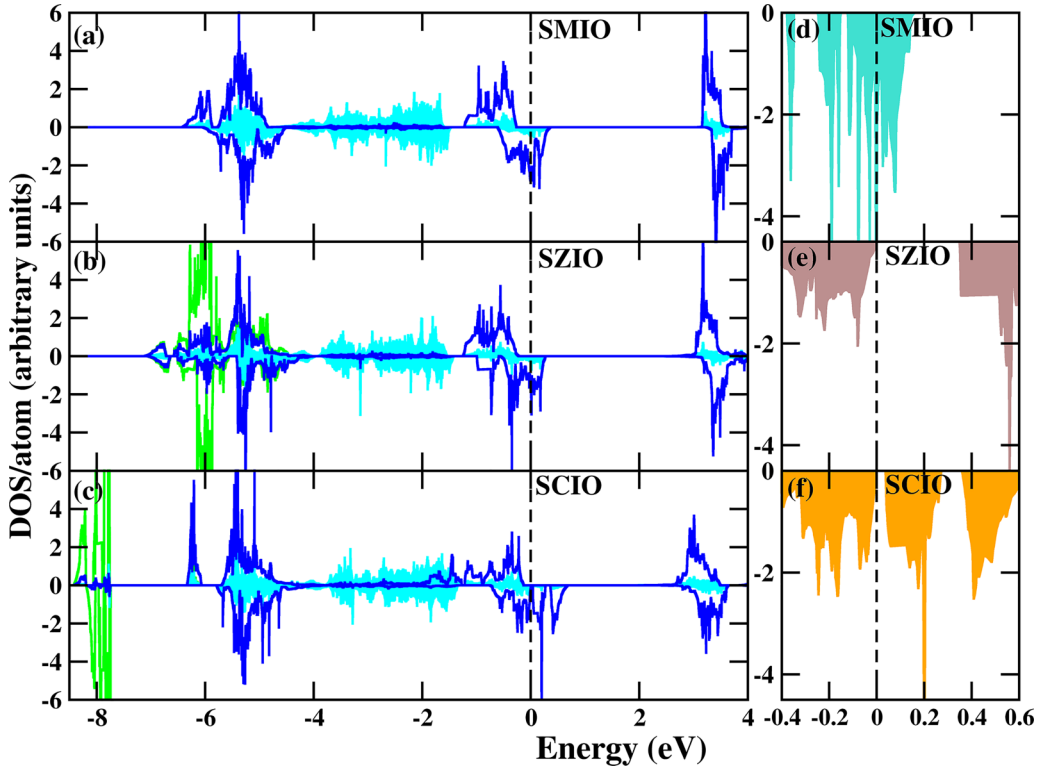

FIG. 2. The left column represents the GGA $+U$ ($U_{\text{eff}} = 2$ eV) density of states for (a) SMIO, (b) SZIO, and (c) SCIO. The Ir-5d and O-2p states are represented by blue and cyan curves, respectively. The green curves represent the Zn-3d and Cd-4d states in (b) and (c), respectively. The density of states in the minority spin channel is shown in the right column for (d) SMIO with GGA + U ($U_{\text{eff}} = 2$ eV) + AFM, (e) SZIO with GGA + U ($U_{\text{eff}} = 3$ eV) + FM, and (f) SCIO with GGA + U ($U_{\text{eff}} = 2$ eV) + FM, which represents the zoomed version of the DOS as shown in (c). The Fermi energy level is set to zero in the energy scale.

whereas Figs. 3(c) and 3(d) depicts the GGA+AFM+SOC and GGA+U+AFM+SOC band structures, where the ground-state AFM ordering has been considered. The 12 bands near the Fermi energy arise from the t_{2g} states of the two Ir sites in the primitive lattice. In Fig. 3(a), the bands overlap at the Fermi energy level near the high-symmetry Γ point. However, as soon as we switch on the electronic correlation (U), a small gap is introduced as shown in Fig. 3(b). The inclusion of the ground-state antiferromagnetic ordering enhances the insulating gap in SMIO. A notable point here is that even in the absence of U, an insulating gap is obtained with AFM configuration as seen in Fig. 3(c). This is majorly due to the reduction of bandwidth in SMIO, driven by AFM exchange. Similar results were previously obtained for isostructural Sr_4IrO_6 [15] and Ca_4IrO_6 [48], where SOC was essential to introduce the insulating state. SOC also has a

TABLE III. The calculated value of spin magnetic moment (in μ_B/site) for GGA+U ($U_{\text{eff}} = 2$ eV) in SMIO (M = Mg, Zn, and Cd).

	SMIO	SZIO	SCIO
Sr	0.00	0.00	0.00
M	0.00	0.01	0.02
Ir	0.61	0.63	0.75
O	0.06	0.06	0.03

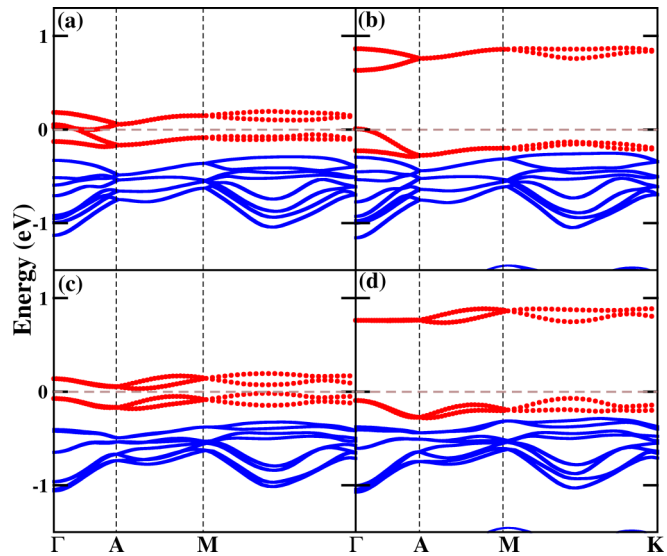

FIG. 3. Ir-5d projected band structure for SMIO along the high-symmetry K points with (a) GGA+FM+SOC [001], (b) GGA+U + FM+SOC [001], (c) GGA+AFM+SOC [001], and (d) GGA+U+AFM+SOC [001]. The blue curves represent the Ir-5d states and the highlighted red curves represent the $j = \frac{1}{2}$ states. The Fermi energy level is set at zero in the energy scale.

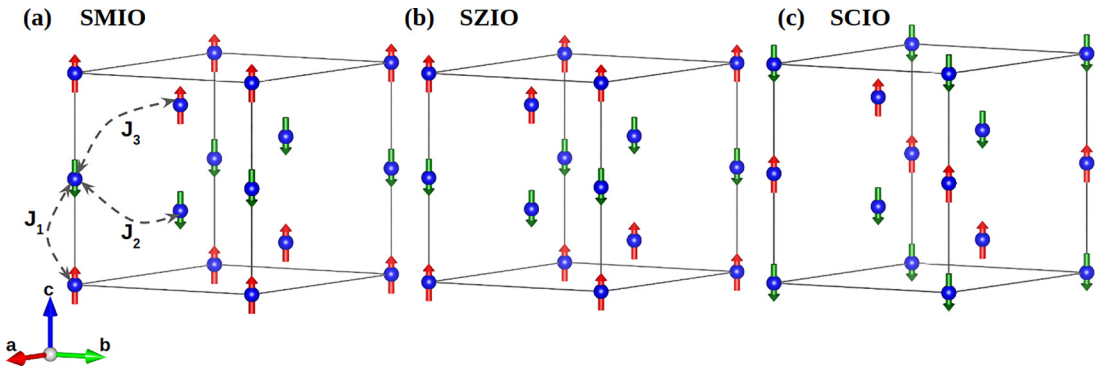

FIG. 4. The magnetic ground state obtained with GGA+U+SOC for (a) SMIO, (b) SZIO, and (c) SCIO. The blue spheres represent the Ir atoms. The red and green arrows represent up and down spins, respectively. The exchange interactions J_1, J_2, and J_3 are marked in (a).

significant influence on the band dispersion of the Ir-5d states for SMIO—the t_{2g} states separate into the $j_{\text{eff}} = \frac{1}{2}$ doublet and the $j_{\text{eff}} = \frac{3}{2}$ quartet. The eight bands arising out of the latter lie in the energy range -0.5 to -1 eV and are completely occupied. The remaining unpaired electrons from the Ir atom goes to the $j_{\text{eff}} = \frac{1}{2}$ doublet and the degeneracy breaks due to partial occupancy. We can visualize the overlapping [Fig. 3(a)] and the well-separated [Fig. 3(c)] $j_{\text{eff}} = \frac{1}{2}$ states near the Fermi energy in SMIO with the FM and ground-state AFM order, respectively. The inclusion of Hubbard correlation U in Figs. 3(b) and 3(d) further separates the $j_{\text{eff}} = \frac{1}{2}$ states, giving rise to completely filled $j_{\text{eff}} = \frac{1}{2}$ lower Hubbard bands and completely empty $j_{\text{eff}} = \frac{1}{2}$ upper Hubbard bands with a gap of the order of 0.6 eV and 0.8 eV, respectively. At this point, we need to emphasize the fact that even in the absence of Coulomb interaction U, SOC transforms SMIO from an AFM metallic to an AFM insulating state. This further denotes the supremacy of SOC interactions which reduces SMIO to a half-filled $j_{\text{eff}} = \frac{1}{2}$ spin-orbit coupled Mott insulator. Here the size of the gap is comparable to the gap size in isostructural Sr_4IrO_6 [15], but much larger as compared to Sr_2IrO_4 [6]. This signifies the importance of the presence of isolated Ir octahedras, which reduces the electronic correlation and enhances the SOC. The point to be noted here is that in Sr_4IrO_6, Ir is in an ideal cubic crystal field, thus intuitively the effect of SOC should be stronger in comparison to SMIO, where Ir occupies a distorted octahedra. However, we find the effect of SOC is similar in both cases, which establishes that SOC indeed is the most crucial interaction in SMIO.

V. MAGNETISM

In this section, we discuss the magnetic ground state of the three systems. Previous studies suggest that the AFM ordering temperature in the case of hexagonal iridates is relatively low compared to other iridate systems due to reduced connectivity among Ir ions [15]. The reduced structural connectivity among the Ir-M-Ir-M chains which host the magnetic Ir site, further reduces the electron hopping integral resulting in limited magnetic exchange. As a starting point, we consider the magnetic unit cell to be the same as the crystallographic hexagonal unit cell and take into account various possible spin configurations to obtain magnetic ground states for SMIO, SZIO, and SCIO as shown in Figs. 4(a)–4(c). The point to be noted here is that in the absence of SOC, we find SMIO and SZIO to be FM in nature. The true AFM ground state in these two compounds could only be realized with the inclusion of SOC, which further indicates the importance of SOC interactions even in deriving the correct magnetic ground state. Our calculations reveal that the spins prefer to orient along the chain axis, i.e., the global z direction in an antiferromagnetic fashion.

To further analyze the nature of the magnetic exchange, we compute the exchange interaction energies. This is implemented by mapping the DFT total energies of several artificially constructed spin configurations into the Heisenberg Hamiltonian [49–51] of the form of, $E^{\text{Tot}} = \sum_{ij} J_{ij} S_i S_j$, where J_{ij} is the magnetic exchange interaction between the ith and jth sites and S_i and S_j are the effective spins at the corresponding sites. There are a few drawbacks of this method, including the choice of correct spin configurations, exchange path, and exchange-correlation functional. Nevertheless, it is known to provide an estimate of the strength and nature of the magnetic exchange interactions, which is much required for qualitative understanding of the magnetic properties of the various classes of materials [35,52–54]. Based on the chainlike structure of the systems, we have considered three independent possible exchange interaction pathways as can be seen in Fig. 4(a). Among them, J_1 represents the Ir-Ir intrachain interaction, whereas J_2 and J_3 are the interchain Ir-Ir interactions among the adjacent chains. J_2 and J_3 take into account the nearest-neighbor (NN) and next-nearest-neighbor (NNN) inter-chain interactions, respectively. The values of the Ir–Ir bond length associated with the various J's is listed in Table IV. The values and nature of the magnetic exchange interaction (J's) considering all the spins to be pointing along the z direction with a spin value of $S = \frac{1}{2}$, is listed in Table IV for SMIO, SZIO, and SCIO.

We find that the intrachain interaction J_1 is uniformly the strongest among all the interactions for SMIO and SCIO as well as SZIO. It is antiferromagnetic in nature, which is crucial in establishing the overall AFM ground state. The point to be noted here is that J_1 is of the same order for SCIO and SZIO, but is almost three times smaller for the case of SMIO. One probable reason could be the presence of d electrons in the closed shell configuration of Cd^{2+} in SCIO and Zn^{2+} in SZIO which aids the electron-hopping. This is, however, not

TABLE IV. The calculated magnetic exchange interactions for different paths for SMIO, SZIO, and SCIO, as shown in Fig. 4(a). The Ir-Ir distance is mentioned in Å and the values of the magnetic exchange interaction in meV.

System	J_1 Ir-Ir distance	(intrachain) value (type)	J_2 Ir-Ir distance	(NN interchain) value (type)	J_3 Ir-Ir distance	(NNN interchain) value (type)
SMIO	5.55	5.784 (AFM)	5.88	0.213 (FM)	6.70	0.014 (AFM)
SZIO	5.60	17.576 (AFM)	5.87	0.391 (FM)	6.70	0.008 (AFM)
SCIO	5.80	16.303 (AFM)	5.90	0.827 (AFM)	6.78	0.008 (AFM)

the scenario in SMIO where the nonmagnetic Mg^{2+} ion is in an open shell configuration. A similar incident has also been previously reported in the case of rock-salt double perovskite (Sr_2BOsO_6; B = Sc, Y, In) [55], where the shell configuration of the nonmagnetic site dictates the strength of the magnetic exchange interactions of the 5d elements. The NN interchain interaction is FM for the case of SMIO and SZIO and AFM for the case of SCIO. However, the strength of J_2 is two orders of magnitude lower compared to J_1. On the other hand, the NNN interaction is almost negligible for all three systems. These findings are crucial in establishing the fact that although the compounds are structurally three-dimensional, nevertheless, from the point of view of magnetic interactions, it reduces to an arrangement of spin-$\frac{1}{2}$ chains along the z direction. Thus, effectively they are quasi-one-dimensional in nature with the absence of any interactions among the consecutive chains. Therefore, it serves as one of the exemplary systems to study the physics of 1D spin chains in the presence of SOC in a j_{eff} basis. Furthermore, from mean-field calculations, we find that the transition temperature for SCIO is of the same order as that of SZIO. For SMIO, our calculations reveal that the transition will occur at a much lower temperature, which is expected to be of the order of $\frac{1}{3}$ value as that of SZIO. These results are consistent with previous experimental findings [38–41].

VI. EFFECT OF SOC

By now, it has been established that SOC is an important energy scale for the compounds under investigation. Hence, a detailed study on its effect becomes inevitable. We thus perform GGA+U+SOC calculations in detail to understand its underlying effects. From Tables III and V, we can see that with the inclusion of SOC, the spin magnetic moment decreases from 0.75 to 0.37 μ_B for SCIO, 0.63 to 0.33 μ_B for SZIO, and 0.61 to 0.31 μ_B for SMIO, and a pronounced orbital magnetic moment occurs at the Ir site with a value of $\sim$0.5 μ_B/site. A large value of the orbital magnetic moment in comparison to its spin counterpart further provides evidence that these systems lie in the strong SOC limit. The μ_{eff} as reported from experimental studies are 1.63, 1.71, and 1.41 for SCIO, SZIO, and SMIO, respectively [38,39]. The point to be noted here is that these values deviate from the ideally expected value of the spin-only magnetic moment of 1.73, with the deviation being much more pronounced in SMIO. The reason becomes prominent from the values of the magnetic moments as obtained from our DFT results, which point out a significant transfer of moment from the spin to the orbital counterpart in the case of SMIO. The ratio of the orbital magnetic moment (o_z) and the spin magnetic moment (m_z), $\frac{o_z}{m_z}$, is found to be largest for SMIO, followed by SZIO and SCIO, thus providing a quantitative analysis of the resultant influence of SOC on these three systems. The $\frac{o_z}{m_z}$ is very high for SMIO ($\sim$1.67), close to the ideally expected value of 2 which is known to occur for strong $j_{\text{eff}} = \frac{1}{2}$ systems [6]. Nevertheless, due to reduced structural connectivity of the IrO_6 octahedras, hexagonal iridates are known to deviate from this ideal behavior [15,37].

The crystal structure of the systems under investigation is highly anisotropic, which further translates to the electronic and magnetic interactions. Hence a high value of MCA energy is intuitive and has also been reported in literature [34,35,56].

TABLE V. The calculated values of spin magnetic moment (m_z) and orbital magnetic moment (o_z) and their ratios are mentioned in the first three columns. The calculations were performed under the GGA+U+SOC scheme along the [001] chain direction. The last column represents the calculated values of magnetocrystalline anisotropy energy for the respective AFM ground states for SMIO, SZIO, and SCIO. The E_{MCA} is calculated as $|E_{||}$-$E_{\perp}|$, where $E_{||}$ and $E_{\perp}$ represent the DFT total energy for the spin configuration parallel and perpendicular chain direction, respectively.

	(m_z) (μ_B/site)	(o_z) (μ_B/site)	$\frac{o_z}{m_z}$	E_{MCA} (meV/f.u)
SMIO	0.31	0.52	1.67	30.44
SZIO	0.33	0.55	1.55	4.48
SCIO	0.37	0.52	1.40	2.66

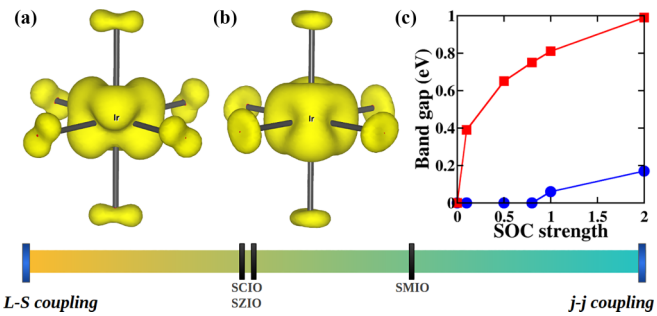

FIG. 5. Density profile of the t_{2g} hole in (a) SZIO and (b) SMIO. (c) The variation of band gap for SMIO due to tuning of SOC strength. The blue and red curves represent the band gaps (in eV) for GGA+AFM+SOC[001] and GGA+U+AFM+SOC[001], respectively.

To estimate the MCA energy and predict the easy axis, we compared the energies along different spin quantization axes, viz. [001] and [110] for the ground-state AFM configuration. Here [001] represents the chain direction and [110] represents the plane perpendicular to the chain direction. We find that in all three cases, the easy axis is towards the crystallographic chain direction, which is expected in a 1D chainlike system [57]. We also counter checked the total energy with a canted spin orientation for all three systems, nevertheless, the spins prefer to orient along the [001] direction. The MCA energies, computed as the energy difference between the easy and the hard axis, which in these three cases are found to be the parallel ($E_{||}$) and perpendicular ($E_{\perp}$) to the chain direction, respectively, are listed in Table V. From our calculations, we infer that the MCA is highest for SMIO with a substantial value of 30.44 meV/f.u. The MCA for SCIO and SZIO are comparable in magnitude and an order of magnitude lower than SMIO. This further highlights the enhanced impact of SOC in SMIO as compared to SCIO and SZIO.

VII. DISCUSSION AND CONCLUSION

The electronic-structure calculation exhibits that SCIO and SZIO with the nonmagnetic sites (Cd and Zn, respectively) in closed shell configuration, fall under the category of a typical correlation-driven Mott insulator. On the other hand, SMIO, where the nonmagnetic site (Mg) is in an open shell electronic configuration, is a SOC-driven Mott insulator. To further shed light on the relative influence of SOC, we look into the density profile of the t_{2g} hole in SZIO and SMIO as shown in Figs. 5(a) and 5(b), respectively. The density profile can be visualized in terms of the magnetization density or the spin density, which represents the shape of the outermost partially occupied orbital. In this case, it reciprocates the t_{2g} hole for the low spin state Ir-5d^5 configuration for both SZIO and SMIO. However, from Figs. 5(a) and 5(b), the density profiles can be observed to be significantly different in both these compounds. For SMIO, the shape of the density hole is closer to what is expected for the ideal $j_{\text{eff}} = \frac{1}{2}$ case [2,10,21]. In SZIO, the spin density is distorted and is more likely to be in an intermediate picture between complete $L - S$ coupling and complete $j - j$ [21] coupling scenarios. This further supports our claim that the effect of SOC is stronger in SMIO with a d^0 configuration as compared to SZIO (or SCIO) with d^{10} configuration. Figure 5(c) represents the variation of the band gap in SMIO, with the modification of the SOC strength. The point to be noted here is that in the presence of Hubbard U, the insulating gap opens up for the SOC strength as low as $\frac{1}{10}$ of the intrinsic value. Thus, for SMIO, the effective SOC strength is higher than the rest and competes with the electronic correlation U.

The strong interplay among electronic correlation, bandwidth, crystal-field splitting, exchange interactions, structural distortion, local geometry, hybridization, and SOC is crucial in understanding the underlying electronic structure and properties of the system. The competition results in the renormalization of the associated energy scales in iridates. This further causes the screening of strong atomic SOC effect, thus resulting in the breakdown of the atomic j-j coupling picture.

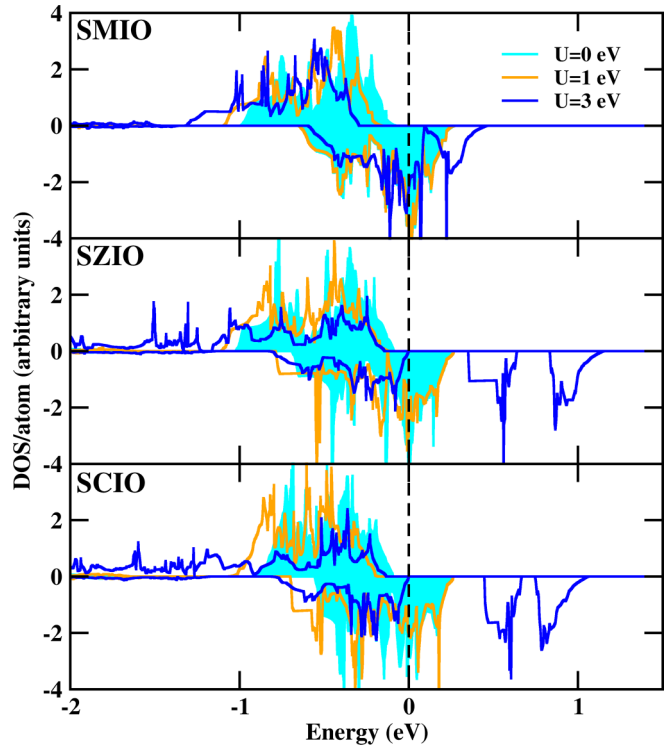

FIG. 6. The calculated GGA+U Ir-5d density of states with the variation of U_{eff} from 0 to 3 eV is shown for SMIO, SZIO, and SCIO in the top, middle, and bottom rows, respectively.

The lattice distortions within the series are quite marginal, which rules it out from being a key ingredient in driving the insulating mechanism. Rather, we believe that the differentiation of SCIO, SZIO, and SMIO, where the first two fall under the category of correlation-driven Mott insulators and the latter as a SOC Mott insulator, is driven by the comparative energetics of relevant energy scales. In the context of our paper, the correlation effects are more predominant in SCIO and SZIO, where the changes in DOS are significant with the variation of U (see Fig. 6). This could be attributed to the fact that unlike SMIO, the nonmagnetic site in SCIO and SZIO consists of $3d/4d$ transition metal ion which accentuates the correlation effects. Another notable point is that the t_{2g} - e_g crystal-field splitting energy increases from SCIO to SZIO to SMIO. From band-structure calculations, we obtain that the t_{2g} bandwidth for SCIO and SZIO is ≈0.9 eV and ≈0.8 eV in SMIO. Then again, for e_g the bandwidth is sufficiently large for SCIO (≈1.7 eV) and SZIO (≈1.6 eV) as compared to SMIO (≈0.9 eV). The combined effects of reduced electronic correlation, large crystal-field splitting, and small bandwidth in SMIO reduce the electronic hopping and push the SMIO to behave closer to that of the atomic j-j-like description as compared to the other two compounds [13]. This can also be traced from the calculated values of magnetic exchange interaction (J's), which are much smaller in SMIO as compared to SCIO and SZIO. The above claims have also been supported by the comparative ratio of the orbital and spin magnetic moment ($\frac{o_z}{m_z}$), which is highest for the SMIO followed by the SZIO and SCIO. All the above conditions support that the strength of effective SOC is much more pronounced in the case of SMIO

than the SZIO and SCIO, however, in all three cases the ideal atomic j-j picture is not a proper description. Rather, they belong to the *intermediate* coupling regime, where SMIO is situated closer to the j_{eff} picture, as shown in the schematic diagram in Fig. 5.

To conclude, using first-principles DFT calculations, we have investigated the electronic structure of three compounds: Sr_3MgIrO_6, Sr_3ZnIrO_6, and Sr_3CdIrO_6. Our study reveals that although these systems are isoelectronic and isostructural, due to the combined influence of crystal structure and crystal field effects, we can differentiate them based on the impact of SOC, which is found to be most crucial for the case of Sr_3MgIrO_6. The evaluated magnetic exchange interactions establish these iridates to be magnetically low dimensional, more precisely, quasi-one-dimensional in nature. Furthermore, the MCA energies were evaluated and a large anisotropy is reported for Sr_3MgIrO_6. Our major findings from the comparative study on the three compounds lead us to believe that technically neither of them are in the ideal j-j coupling regime, however, SMIO is the closest to the ideal atomic j-j picture. We hope our theoretical results will stimulate further experimental investigations on these systems.

ACKNOWLEDGMENTS

We thank I. Dasgupta for fruitful discussions. R.R. thanks IIT Goa for providing research fellowship.

APPENDIX

In the three hexagonal perovskites under discussion, the nonmagnetic sites consist of elements spanning various groups of the periodic table. Although uncanny, previously it has been seen that the nonmagnetic site could also impact the electronic and magnetic properties of the system. The significant difference among the nonmagnetic sites is the presence of $3d/4d$ transition metal atoms in SZIO and SCIO. Since in transition metals the electron-electron correlation is sizable, we study its influence on the hexagonal iridates by tuning the value of the Hubbard U parameter. The evolution of the density of states thus obtained is shown in Fig. 6.

[1] W. Witczak-Krempa, G. Chen, Y. B. Kim, and L. Balents, Annu. Rev. Condens. Matter Phys. **5**, 57 (2014).
[2] J. G. Rau, E. Kin-Ho Lee, and H. Y. Kee, Annu. Rev. Condens. Matter Phys. **7**, 195 (2016).
[3] K. S. Pedersen, J. Bendix, A. Tressaud, E. Durand, H. Weihe, Z. Salman, T. J. Morsing, D. N. Woodruff, Y. Lan, W. Wernsdorfer, C. Mathonie, S. Piligkos, S. I. Klokishner, S. Ostrovsky, K. Ollefs, F. Wilhelm, A. Rogalev, and R. Clérac, Nat. Commun. **7**, 12195 (2016).
[4] G. Cao and P. Schlottmann, Rep. Prog. Phys. **81**, 042502 (2018).
[5] S. Bhowal and I. Dasgupta, J. Phys.: Condens. Matter **33**, 453001 (2021).
[6] B. J. Kim, H. Jin, S. J. Moon, J. Y. Kim, B.-G. Park, C. S. Leem, J. Yu, T. W. Noh, C. Kim, S. J. Oh, J. H. Park, V. Durairaj, G. Cao, and E. Rotenberg, Phys. Rev. Lett. **101**, 076402 (2008).
[7] B. J. Kim, H. Ohsumi, T. Komesu, S. Sakai, T. Morita, H. Takagi, and T. Arima, Science **323**, 1329 (2009).
[8] F. Wang and T. Senthil, Phys. Rev. Lett. **106**, 136402 (2011).
[9] X. Wan, Ari M. Turner, Ashvin Vishwanath, and Sergey Y. Savrasov, Phys. Rev. B **83**, 205101 (2011).
[10] G. Jackeli and G. Khaliullin, Phys. Rev. Lett. **102**, 017205 (2009).
[11] S. J. Moon, H. Jin, K. W. Kim, W. S. Choi, Y. S. Lee, J. Yu, G. Cao, A. Sumi, H. Funakubo, C. Bernhard, and T. W. Noh, Phys. Rev. Lett. **101**, 226402 (2008).
[12] G. Cao, T. F. Qi, L. Li, J. Terzic, S. J. Yuan, L. E. DeLong, G. Murthy, and R. K. Kaul, Phys. Rev. Lett. **112**, 056402 (2014).
[13] S. Bhowal, S. Baidya, I. Dasgupta, and T. Saha-Dasgupta, Phys. Rev. B **92**, 121113(R) (2015).
[14] T. Dey, A. Maljuk, D. V. Efremov, O. Kataeva, S. Gass, C. G. F. Blum, F. Steckel, D. Gruner, T. Ritschel, A. U. B. Wolter, J. Geck, C. Hess, K. Koepernik, J. van den Brink, S. Wurmehl, and B. Buchner, Phys. Rev. B **93**, 014434 (2016).
[15] X. Ming, X. Wan, C. Autieri, J. Wen, and X. Zheng, Phys. Rev. B **98**, 245123 (2018).
[16] A. Nag, S. Bhowal, M. Moretti Sala, A. Efimenko, I. Dasgupta, and S. Ray, Phys. Rev. Lett. **123**, 017201 (2019)
[17] M. S. Khan, C. Meneghini, F. Bert, M. M. Sala, and S. Ray, Phys. Rev. B **104**, 214414 (2021).
[18] A. Bandyopadhyay, A. Chakraborty, S. Bhowal, V. Kumar, M. M. Sala, A. Efimenko, C. Meneghini, I. Dasgupta, T. Saha Dasgupta, A. V. Mahajan, and S. Ray, arXiv:2111.00925.
[19] A. Bandyopadhyay, A. Chakraborty, S. Bhowal, Vinod Kumar, M. M. Sala, A. Efimenko, F. Bert, P. K. Biswas, C. Meneghini, N. Büttgen, I. Dasgupta, T. Saha Dasgupta, A. V. Mahajan, and S. Ray, Phys. Rev. B **105**, 104431 (2022).
[20] D. I. Khomskii, *Transition Metal Compounds* (Cambridge University Press, Cambridge, 2014).
[21] S. Kanungo, K. Mogare, B. Yan, M. Reehuis, A. Hoser, C. Felser, and M. Jansen, Phys. Rev. B **93**, 245148 (2016).
[22] X. Liu, V. M. Katukuri, L. Hozoi, W. G. Yin, M. P. M. Dean, M. H. Upton, J. Kim, D. Casa, A. Said, T. Gog, T. F. Qi, G. Cao, A. M. Tsvelik, J. van den Brink, and J. P. Hill, Phys. Rev. Lett. **109**, 157401 (2012).
[23] W.-G. Yin, X. Liu, A. M. Tsvelik, M. P. M. Dean, M. H. Upton, Jungho Kim, D. Casa, A. Said, T. Gog, T. F. Qi, G. Cao, and J. P. Hill, Phys. Rev. Lett. **111**, 057202 (2013).
[24] G. L. Stamokostas and G. A. Fiete, Phys. Rev. B **97**, 085150 (2018).
[25] J. C. Leiner, J. Oh, A. I. Kolesnikov, M. B. Stone, M. D. Le, E. P. Kenny, B. J. Powell, M. Mourigal, E. E. Gordon, M. H. Whangbo, J. W. Kim, S. W. Cheong, and Je-Geun Park, Phys. Rev. B **97**, 104426 (2018).
[26] S. Toth, W. Wu, D. T. Adroja, S. Rayaprol, and E. V. Sampathkumaran, Phys. Rev. B **93**, 174422 (2016).
[27] E. V. Sampathkumaran, N. Mohapatra, S. Rayaprol, and K. K. Iyer, Phys. Rev. B **75**, 052412 (2007).
[28] A. D. Hillier, D. T. Adroja, W. Kockelmann, L. C. Chapon, S. Rayaprol, P. Manuel, H. Michor, and E. V. Sampathkumaran, Phys. Rev. B **83**, 024414 (2011).

[29] V. K. Anand, D. T. Adroja, S. Rayaprol, A. D. Hillier, J. Sannigrahi, M. Rotter, M. D. Le, and E. V. Sampathkumaran, Phys. Rev. B **108**, 144426 (2023).
[30] V. Eyert, U. Schwingenschlögl, R. Frésard, A. Maignan, C. Martin, N. Nguyen, C. Hackenberger, and T. Kopp, Phys. Rev. B **75**, 115105 (2007).
[31] S. Niitaka, K. Yoshimura, K. Kosuge, M. Nishi, and K. Kakurai, Phys. Rev. Lett. **87**, 177202 (2001).
[32] E. V. Sampathkumaran and A. Niazi, Phys. Rev. B **65**, 180401(R) (2002).
[33] Y. J. Choi, H. T. Yi, S. Lee, Q. Huang, V. Kiryukhin, and S. W. Cheong, Phys. Rev. Lett. **100**, 047601 (2008).
[34] D. Mikhailova, B. Schwarz, A. Senyshyn, A. M. T. Bell, Y. Skourski, H. Ehrenberg, A. A. Tsirlin, S. Agrestini, M. Rotter, 1 P. Reichel, J. M. Chen, Z. Hu, Z. M. Li, Z. F. Li, and L. H. Tjeng, Phys. Rev. B **86**, 134409 (2012).
[35] S. Sarkar, S. Kanungo, and T. Saha-Dasgupta, Phys. Rev. B **82**, 235122 (2010).
[36] T. Birol, K. Haule, and D. Vanderbilt, Phys. Rev. B **98**, 134432 (2018).
[37] X. Ou and H. Wu, Sci. Rep. **4**, 4609 (2014).
[38] N. Segal, J. F. Vente, T. S. Bush, and P. D. Battle, J. Mater. Chem. **6**, 395 (1996).
[39] P. Nuñez, S. Trail, and H. Zur Loye, J. Solid State Chem. **130**, 35 (1997).
[40] C. Lampe-Önnerud, M. Sigrist, and H.-C. Zur Loye, J. Solid State Chem. **127**, 25 (1996).
[41] P. A. McClarty, A. D. Hillier, D. T. Adroja, D. D. Khalyavin, S. Rayaprol, P. Manuel, W. Kockelmann, and E. V. Sampathkumaran, J. Phys. Soc. Jpn. **89**, 064703 (2020).
[42] J. P. Perdew, K. Burke, and M. Ernzerhof, Phys. Rev. Lett. **77**, 3865 (1996).
[43] G. Kresse and J. Hafner, Phys. Rev. B **47**, 558(R) (1993).
[44] G. Kresse and J. Furthmüller, Phys. Rev. B **54**, 11169 (1996).
[45] V. I. Anisimov, I. V. Solovyev, M. A. Korotin, M. T. Czyzyk, and G. A. Sawatzky, Phys. Rev. B **48**, 16929 (1993).
[46] S. L. Dudarev, G. A. Botton, S. Y. Savrasov, C. J. Humphreys, and A. P. Sutton, Phys. Rev. B **57**, 1505 (1998).
[47] D. Hobbs, G. Kresse, and J. Hafner, Phys. Rev. B **62**, 11556 (2000).
[48] S. Calder, G.-X. Cao, S. Okamoto, J. W. Kim, V. R. Cooper, Z. Gai, B. C. Sales, M. D. Lumsden, D. Mandrus, and A. D. Christianson, Phys. Rev. B **89**, 081104(R) (2014).
[49] C. S. Helberg, W. E. Pickett, L. L. Boyer, H. T. Stokes, and M. J. Mehl, J. Phys. Soc. Jpn. **68**, 3489 (1999).
[50] V. V. Mazurenko, F. Mila, and V. I. Anisimov, Phys. Rev. B **73**, 014418 (2006).
[51] H. J. Xiang, E. J. Kan, S. H. Wei, M. H. Whangbo, and X. G. Gong, Phys. Rev. B **84**, 224429 (2011).
[52] S. Kanungo, B. Yan, M. Jansen, and C. Felser, Phys. Rev. B **89**, 214414 (2014).
[53] J. Sannigrahi, J. Sichelschmidt, B. Koo, A. Banerjee, S. Majumdar, and S. Kanungo, J. Phys.: Condens. Matter **31**, 245802 (2019).
[54] R. Roy and S. Kanungo, Phys. Rev. B **106**, 125113 (2022).
[55] S. Kanungo, B. Yan, C. Felser, and M. Jansen, Phys. Rev. B **93**, 161116(R) (2016).
[56] Hua Wu, M. W. Haverkort, Z. Hu, D. I. Khomskii, and L. H. Tjeng, Phys. Rev. Lett. **95**, 196404 (2005).
[57] E. Lefrançois, L. C. Chapon, V. Simonet, P. Lejay, D. Khalyavin, S. Rayaprol, E. V. Sampathkumaran, R. Ballou, and D. T. Adroja, Phys. Rev. B **90**, 014408 (2014).